

# 1 **Experimental and numerical identification of corrosion degradation of ageing structural** 2 **components**

3 Beata Zima<sup>a</sup>, Krzysztof Wołoszyk<sup>a</sup>, Yordan Garbatov<sup>b, 1</sup>

4 <sup>a</sup> *Institute of Ocean Engineering and Ship Technology, Gdansk University of Technology,*  
5 *G. Narutowicza 11/12 st., 80-233 Gdansk, Poland*

6 <sup>b</sup> *Centre for Marine Technology and Ocean Engineering (CENTEC), Instituto Superior Técnico,*  
7 *Universidade de Lisboa, Avenida Rovisco Pais 1049-001 Lisboa, Portugal*

## 8 **Abstract**

9 The study presents experimental and numerical identification of corrosion degradation of thin-  
10 walled structural components employing guided wave propagation. The steel structural  
11 components are subjected to through-thickness varying corrosion degradation levels. The  
12 developed approach using the non-destructive guided wave-propagation quantifies the  
13 equivalent average corrosion degradation level exploring a limited number of transducers. A  
14 group velocity dispersion curve reconstruction has been used to determine the corrosion-  
15 induced plate thickness reduction. Two case studies are used to examine experimentally the  
16 newly developed approach. In the first one, the dispersion curve and the assessment of the  
17 corrosion thickness reduction have been made using wave signals of various excitation  
18 frequencies. In the second one, the analysis has been conducted only for two wave propagation  
19 signals and one excitation frequency which allowed for reconstructing the dispersion curve in  
20 a limited frequency range. In both case studies, a good agreement between the natural and  
21 estimated corrosion degradation levels was observed. The present study develops a signal  
22 processing methodology, which can be used in the SHM systems, where several aspects still  
23 need to be further investigated before it can be applied in large size and complex geometry of  
24 ship hull structures.

## 25 **Keywords:**

26 corrosion degradation; steel plates; ship structures; NDT; ultrasonic waves

## 27 **1 Introduction**

28 Ships and offshore structures are operating in a highly corrosive environment. The  
29 excessive corrosion degradation may lead to catastrophic consequences, e.g., exceedance of the

---

<sup>1</sup> Corresponding author e-mail: [yordan.garbatov@tecnico.ulisboa.pt](mailto:yordan.garbatov@tecnico.ulisboa.pt); Telf (351) 21 841 7907

30 ultimate strength of ship structural components (Woloszyk et al., 2018) and entire ship hull  
31 (Parunov et al., 2007). According to Zayed et al. (Zayed et al., 2018), even up to 90% of ship  
32 hull damages are primarily or indirectly caused by corrosion. An example of tanker ship loss,  
33 mainly driven by excessive corrosion degradation, breaking the ship's hull in two parts, is the  
34 tanker Prestige in 2002 (Flashback history: Tanker Prestige sinking (Video), 2015).

35 There are regular surveys of the entire ship to avoid severe degradation, where the  
36 thickness of structural components is measured using an ultrasonic thickness gauge. This  
37 method has various advantages, i.e., the equipment is portable, and the usage is user-friendly.  
38 However, it provides information about thickness in one point of any particular measurement.  
39 Thus, numerous thickness measurements must be done to correctly map the distribution of  
40 thickness corrosion diminutions within larger structures like ship hulls.

41 Cegla and Gajdacs (Cegla and Gajdacs, 2016) found that irregularities in corroded  
42 surfaces disturb the ultrasonic measurements and usually overestimate the corroded plate  
43 thickness value. Similar observations have been found in (Woloszyk et al., 2021). Zayed et al.  
44 (Zayed et al., 2008) analysed the factors that may disturb the ultrasonic measurements, e.g.  
45 lighting, cleanliness and accessibility to the inspected area. Additionally, there is always a  
46 probability that some deteriorated structural components are omitted during the inspections.  
47 Such a possibility may be seen in a more difficult area for inspection as double bottom or closed  
48 spaces.

49 To reflect some problems faced with using the non-destructive measuring techniques,  
50 some new approaches were developed, especially based on guided waves, which were proved  
51 to be very useful in diagnostics of both localized damages (Cao et al., 2021; Wandowski et al.,  
52 2011; Zima, 2021), as well as surface damages (Ding et al., 2021; Hu et al., 2022; Zima and  
53 Rucka, 2017). The guided wave propagation seems to define the corrosion degradation level  
54 around the structural components effectively. The most advantageous feature of the guided  
55 wave propagation approach is mapping a larger area of the thickness of structural components.  
56 Moreover, high-frequency wave-based methods are generally insensitive to applied loads and  
57 low-stress levels (the differences in wave velocities are negligible), which significantly  
58 facilitates the analysis and results interpretation (Li et al., 2021).

59 Ervin and Reis (Ervin and Reis, 2008) tested the guided waves' low and high-frequency  
60 ranges to monitor the reinforced bar's corrosion degradation in mortar specimens. Ervin et al.  
61 (Ervin et al., 2009) used longitudinal ultrasonic waves of high frequencies to monitor the  
62 reinforced mortar specimens undergoing accelerated uniform and localised corrosion.

63 Two ultrasonic techniques of pulse transmission and pulse-echo were used to monitor the  
64 healthy and damaged bar by Sharma and Mukherje (Sharma and Mukherjee, 2010). Fractal  
65 analysis of guided ultrasonic waves for evaluating the corrosion degradation level in post-  
66 tensioned systems was proposed by Moustafa et al. (Moustafa et al., 2014). Farhidzadeh and  
67 Salamone (Farhidzadeh and Salamone, 2015) used dispersion curves, continuous wavelet  
68 transform, and wave velocity measurement to quantify the corrosion damage of multiwire  
69 prestressing steel strands.

70 In all reported cases, the corrosion degradation was accelerated by applying the direct  
71 current. The level of corrosion degradation (mass loss) was linearly dependent on corrosion  
72 current and time elapsed. The corrosion degradation assessment was based on the analysis of  
73 the dispersion curves. Because the shape of dispersion curves mainly depends on the geometric  
74 parameters, monitoring the trace changes efficiently assessed the corrosion degradation level.

75 Recently the methods of dispersion curve reconstruction have been extensively studied.  
76 However, the dispersion curve reconstruction demands multiple measurements along the  
77 relatively short propagation path, which would be inefficient in a large-scale structure like  
78 offshore platforms or ships (Draudviliene et al., 2021). Finally, there are almost no studies  
79 regarding guided wave propagation to identify the corrosion degradation of thin-walled  
80 structures subjected to environmental corrosion. Most of the studies were related to localised  
81 pitting corrosion (Ciampa et al., 2015; Ding et al., 2021; Howard and Cegla, 2017; Hua et al.,  
82 2020; Tian et al., 2021). The corrosion degradation observed in ship structures is mainly general  
83 (Panayotova and Garbatov, 2010), although pitting one is quite common too. General corrosion  
84 is observed, e.g., in cargo holds as well as in ballast tanks.

85 Recently, the study aimed at a corrosion assessment using the guided ultrasonic waves  
86 (Zima et al., 2022), contained a detailed description of a methodology based on the phase  
87 velocity and convex optimization. The study performed here is the next step aimed at procedure  
88 simplification and reducing the extent of the sensors network, as well as the collected data in  
89 the future SHM systems. Previously employed phase velocity was determined using spectral  
90 decomposition and the zero-cross method. Because of the dispersive nature of guided waves  
91 and spreading the wave packet, the unambiguous identification of corresponding roots may be  
92 associated with impediments to interpretation. Moreover, it was proved that usually the phase  
93 velocity is overestimated which leads to underestimation of corrosion degradation level [20].  
94 Therefore, in the following study, the approach based on dispersion curve reconstruction has  
95 been modified and we have used the Hilbert transform and group velocity curve to assess the  
96 degradation level of thin-walled ship structures. Such modifications allow for simplification of



97 the signal processing procedure. The newly developed approach's main advantage is that only  
98 two adjacent wave propagation signals are needed in the identification process. The limited  
99 number of essential signals processed within the algorithm is extremely important from the  
100 point of view of the further development of the diagnostics systems and data communication.  
101 The smaller number of signals requires fewer measurements which in turn means a smaller size  
102 of memory and the whole size of the potential devices. Additionally, the smaller size of the  
103 device and a limited number of excitations and registrations entail longer battery life and lower  
104 costs of equipment maintenance. Although the presented algorithm is only the first step in the  
105 development of the diagnostics methods for ship structural monitoring and its requirement  
106 improvements which are faithfully discussed in the paper, the small amount of necessary data  
107 is one of its most significant advantages.

108 The corrosion degradation level of a significant area may be assessed, which makes the  
109 newly developed approach far more effective than the standard one of the ultrasonic thickness  
110 measurement or wave tomography. The analysed corroded thin-walled structural components  
111 were initially corroded employing an originally designed corrosion deterioration set-up. The  
112 corrosion degradation process was in line with in-situ environmental degradation. The designed  
113 corrosion deterioration set-up has a significant advantage over the efficient DC-induced  
114 corrosion degradation and leads to more realistic surface characteristics (Xiao et al., 2020; Yuan  
115 et al., 2007), but is still very different from the real one.

116 Based on the obtained reconstructed dispersion curves the corrosion degradation level has  
117 been assessed. To analyse the effectiveness and accuracy of state assessment of the specimen,  
118 the analysis stage has been divided into two stages. Within the first stage, five different  
119 frequencies were used in the study and the curves have been reconstructed in the wide frequency  
120 range. At the second stage, the curve was traced only for a narrow frequency range  
121 reconstructed after one excitation. In both cases, the progress of corrosion degradation affected  
122 the shape of the curves. The results collected within both stages were compared with the actual  
123 one determined by mass calculation. The agreement between the results suggests the potential  
124 of the novel method in corrosion degradation monitoring. The article discusses both advantages  
125 and disadvantages of the proposed method.



## 126 2 Guided waves propagation in thin-walled structures

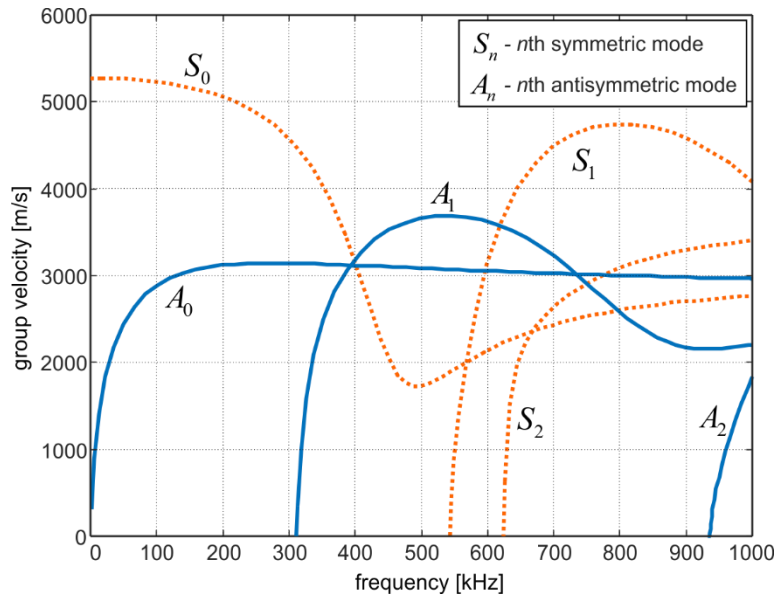
### 127 2.1 Theoretical background

128 The guided waves in plates are generated due to the interaction of compressive and shear  
129 waves propagating in elastic, homogeneous, isotropic medium bounded with two equidistant  
130 surfaces. Horace Lamb foresaw their existence (Lamb, 1917) and derived dispersion equations  
131 relating to the propagation velocity and the number of possible wave modes with an excitation  
132 frequency. In general, the Lamb waves can exist as symmetric and antisymmetric. They are  
133 high dispersive, and their propagation velocity depends on the frequency and plate thickness  
134 product. Two equations describe the dispersive characteristics of both types:

$$135 \frac{\tan(qd)}{\tan(pd)} = -\frac{(k^2 - q^2)^2}{4k^2 pq}, \quad (1a)$$

$$136 \frac{\tan(qd)}{\tan(pd)} = -\frac{4k^2 pq}{(k^2 - q^2)^2} \quad (1b)$$

137 where  $d$  is the plate thickness and the parameters  $p$  and  $q$  depend on wavenumber  $k$ , angular  
138 frequency  $\omega$ , longitudinal wave velocity ( $c_L$ ) or shear wave velocity ( $c_T$ ) in the infinite  
139 medium. The velocities of guided and bulk waves depend also on the material parameters of  
140 the considered medium. Eqn 1a is associated with symmetric particle motion about the  
141 midplane, while Eqn 1b describes the antisymmetric particle motion caused by wave  
142 propagation. The number of possible solutions fulfilling the Eqn (1) is infinite, and in general,  
143 the roots may be complex. However, the real roots are associated with propagating waves, while  
144 imaginary roots corresponding to evanescent waves will not be considered in further analysis.  
145 The solution of the dispersion equation is presented in the form of dispersion curves. At least  
146 one symmetric mode (S) resembling axial waves and one antisymmetric mode (A) resembling  
147 flexural wave exists for each frequency. The number of possible curves associated with any  
148 particular wave mode increases with the increase of the considered frequency range. The  
149 exemplary dispersion curves traced for a steel plate are presented in Figure 1.



150

151  
152

Figure 1 Dispersion curves for a steel plate with a thickness of 5 mm, elastic modulus  $E = 198$  GPa,  $\nu = 0.3$  and density  $7,850$  kg/m<sup>3</sup>

153

154

155

156

157

158

159

It has to be pointed out that the Lamb theory is valid only for plates with constant thickness, and their material fulfils the conditions of elasticity, homogeneity, and isotropy. Meanwhile, the corroded specimens are usually covered with corrosion products varying in mechanical properties from the undamaged core. In general, the additional layers require different wave theories, but in the following study, the corrosion products were removed before the investigation to assess the damage degradation level. This research will verify the correctness of the assumption about the constant thickness.

160

## 2.2 Signal processing procedure

161

162

163

164

165

166

167

168

169

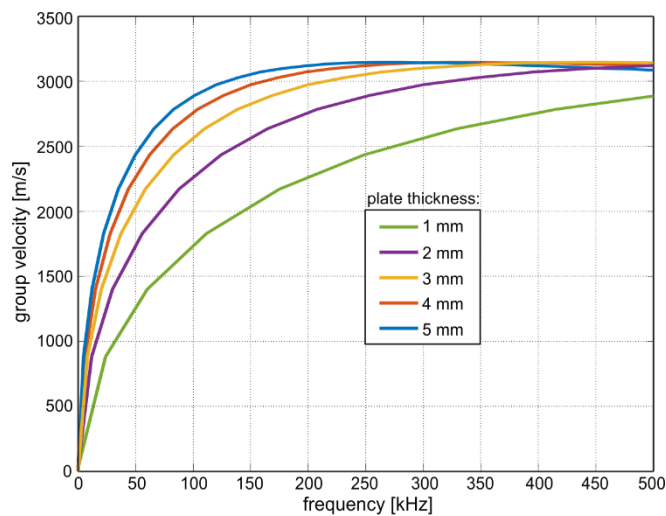
170

171

As mentioned, the shape of dispersion curves depends on the material and geometric parameters of the considered plate. The proposed approach for a corrosion level assessment assumes that corrosion degradation influences the thickness of the plate. At the same time, the elastic modulus, density, and Poisson's ratio are considered to remain unaffected. In consequence, the shape of the dispersion curve depends on the corrosion deterioration level. In general, the assumption about the constant material parameters is not valid for cases of corroded structures and will be verified in this study. However, the plate thickness is the most influential factor, and its variation affects the wave velocity the most. Figure 2 presents the dispersion curve associated with the first antisymmetric Lamb mode in the frequency range (0-500 kHz) for steel plates with varying thicknesses. For some frequencies, the degree in the group propagation velocities is significant (i.e., 100 kHz). In contrast, for some frequencies, the curves

172 coincide with each other, which indicates that the corrosion degradation (plate thickness  
173 reduction) does not impact the wave propagation (i.e., 400-500 kHz).

174



175

176 Figure 2 Dispersion curve associated with the first antisymmetric Lamb mode for plates with a varying thickness

177

178 Moreover, the corrosion degradation impact depends on the initial parameters of the  
179 uncorroded plate. One-millimetre thickness reduction in a plate with an initial thickness of 5  
180 mm results in an insignificant change in the dispersion curve shape. In contrast, in the case of  
181 thinner plates, the difference is noticeable. There is no explicitly given relationship between the  
182 frequency, propagation velocity, and thickness reduction. However, for every thickness,  
183 frequencies of corrosion damage can be identified. The newly developed approach here aims to  
184 reconstruct the dispersion curve representing group velocity, enabling a better estimation of the  
185 average plate thickness during corrosion degradation.

186

187 The corrosion degradation level identification is based on measuring at least two signals  
188 by the transducers attached at two distinct positions. The distance between the actuator and  
189 sensors should be established by taking into account the dispersive nature of guided waves,  
190 signal attenuation, the energy of the input wave, and the size of the area, which is monitored.  
191 The shorter distance results in a greater signal-to-noise ratio (SNR), which facilitates the  
192 interpretation of the results. The longer distance allows for assessing a greater area of the tested  
193 structure.

194

195 The algorithm presented here aimed at the reconstruction of dispersion curves using  
196 adjacent signals has been also analysed and utilized by other researchers (Draudviliene et al.,  
197 2021; Zima et al., 2022). The main development is its modification for group velocity extraction  
and employment in the corrosion degradation assessment. For clarity, a brief description of the  
following steps is presented here.

198 In the first step of the developed approach, the guided Lamb waves are excited by an  
 199 actuator triggering a narrowband burst. In this study, the five-cycle sinusoid modulated by the  
 200 Hann window is used (Lyons, 2011):

$$201 \quad p(t) = \begin{cases} p_0 \sin(2\pi ft) \cdot w(t) & t \in [0, T_w] \\ 0 & t \geq T_w \end{cases}, \quad (2)$$

202 where  $f$  is the excitation frequency,  $p_0$  denotes the excitation amplitude, and  $T_w$  is the modulating  
 203 window length. The modulation window is described by a function:

$$204 \quad w(t) = 0.5 \left( 1 - \cos \left( \frac{2\pi ft}{n_w} \right) \right), \quad t \in [0, T_w], \quad (3)$$

205 Next, the incident waves captured by sensors are identified and extracted from the  
 206 adjacent signals (Figure 3, stage II). The reflections from the edges or other obstacles registered  
 207 further in the signal are not considered, significantly simplifying the analysis, which is one of  
 208 the most important advantages of this approach, especially in the context of the further research  
 209 dedicated to diagnostics of large and complex structures. The trigonometric representations of  
 210 the incident waves are calculated using the Fourier integral and the frequency response  
 211 amplitude (Figure 3, stage III). The spectrum is normalised as the maximum value equals 1.0  
 212 in each case (Figure 3, stage IV). Based on the frequency ranges of the obtained spectra, the  
 213 frequency limits  $f_L$  and  $f_H$  are established. In general, the spectrum vanishes above the upper-  
 214 frequency limit  $f_H$  and below the lower frequency limit  $f_L$  (Figure 3, stage V). Regardless of  
 215 the spectra' differences for signals registered during the same measurement, the frequency limits  
 216 are the same. Next, the frequency spectra  $S(f)$  are filtered by using  $n$  bandpass filters defined  
 217 as a Gaussian magnitude function:

$$218 \quad U_k(f) = S(f) B_k(f) = S(f) e^{4 \ln(0.5) \left( \frac{f - f_L - (k-1) \Delta f}{\Delta B} \right)^2}, \quad (4)$$

219 and  $k=1, 2, \dots, n$ . According to recommendations formulated by He (Ping He, 1998), the number  
 220 of filters  $n$  depends on the bandwidth parameter  $\Delta B$ , which defines the frequency range limited  
 221 by the single filter:

$$222 \quad n > 1 + \frac{f_H - f_L}{\Delta B}, \quad (5)$$

223 Here, the bandwidth parameter  $\Delta B$  was determined based on the normalised Fourier  
 224 frequency spectrum. Its value was established based on the spectrum width for the normalised  
 225 amplitude corresponding to the -3dB value. In the next stage, the signal is synthesised from the  
 226 basic trigonometric functions by using the inverse Fourier transform (Figure 3, stage VI).



227 Finally, the time of flight was determined by the envelope method. The envelope of the signal  
228 was calculated using the Hilbert transform (Figure 3, stage VII and VIII). The time of flight  
229 was computed using the cross-correlation method and was defined as the peak-to-peak value.  
230 The group velocity of Lamb waves was calculated as the distance  $x$  divided by the time of the  
231 flight. The shape of the dispersion curve was reconstructed by plotting the set of frequencies  
232 and corresponding group velocities (Figure 3, stage IX). Employing the group velocity instead  
233 of the phase velocity as a quality indicator significantly facilitates the robustness of the  
234 developed procedure.

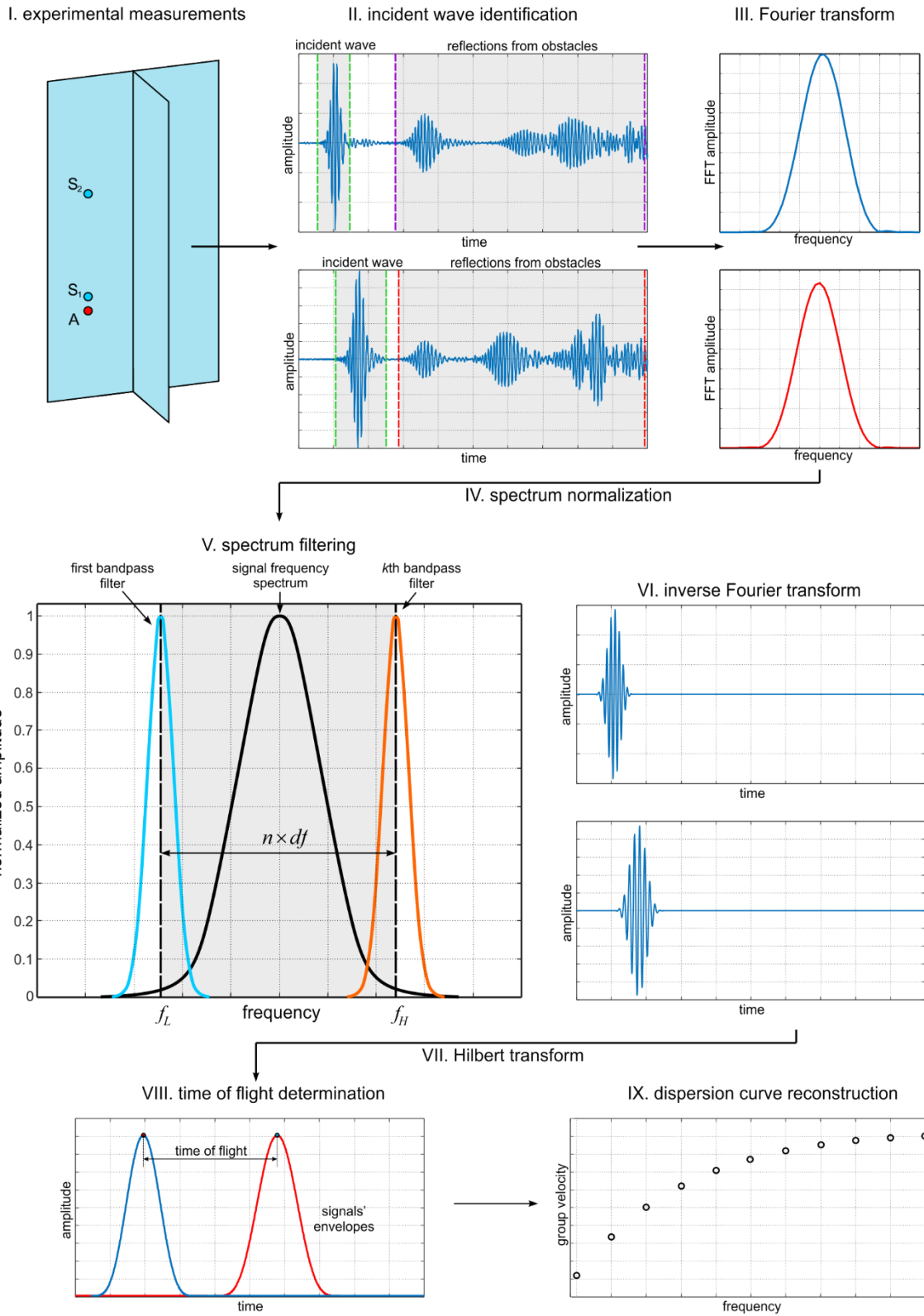
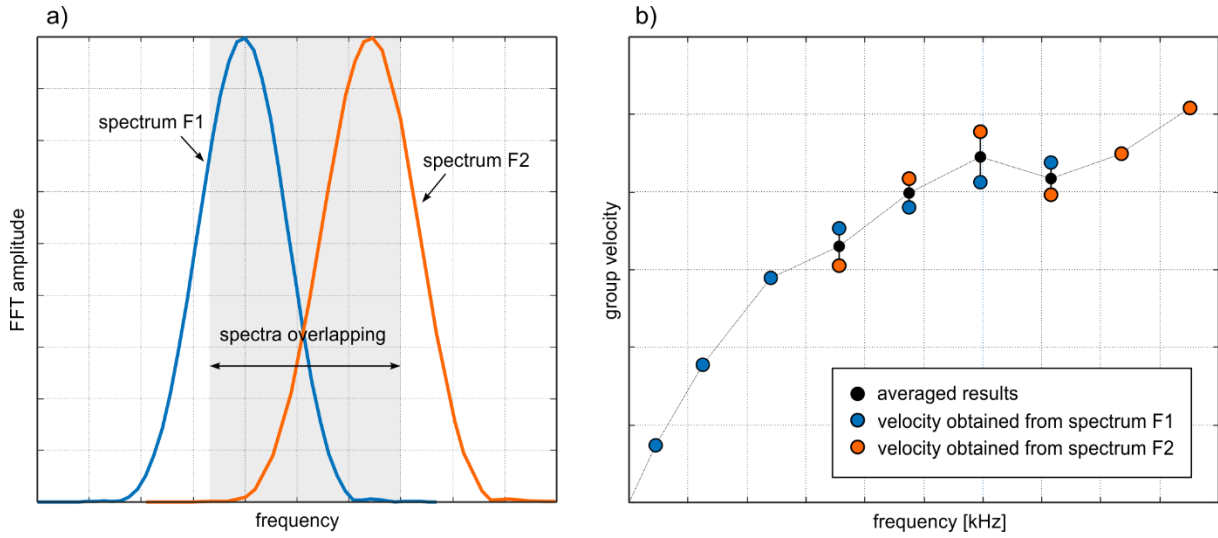


Figure 3 Signal processing procedure

The frequency range within the shape of the dispersion curve can be reconstructed based on the excitation frequency, the width of the signal spectrum, and spectra frequency limits  $f_L$  and  $f_H$ . In general, the segments of dispersion curves obtained for various frequencies may

235  
236  
237  
238  
239

240 overlap (Figure 4a). In such a case, the procedure has been extended by an additional step, and  
 241 the group velocity was averaged within the common frequency region (Figure 4b).



242  
 243 Figure 4 Processing of experimental data: a) spectra overlapping and b) averaging of group velocity determined  
 244 in a common frequency range of both spectra

### 245 2.3 Identification of corrosion degradation level

246 To estimate the thickness reduction based on the reconstructed dispersion curve, first, the  
 247 dependence for the first antisymmetric Lamb mode  $A_0$  was calculated for the pre-established  
 248 plate thickness  $d$ . Then, the dispersion curve determined numerically based on the analytical  
 249 equation was considered as the sets of  $n$  pairs of numbers:

$$250 \quad c_{gr}^T(d) = \{(\Delta f, c_{gr}^T(\Delta f)), (2\Delta f, c_{gr}^T(2\Delta f)), \dots, (n\Delta f, c_{gr}^T(n\Delta c_{gr}))\} = \{(\Delta f, c_{gr}^{T,1}), (2\Delta f, c_{gr}^{T,2}), \dots, (n\Delta f, c_{gr}^{T,n})\}$$

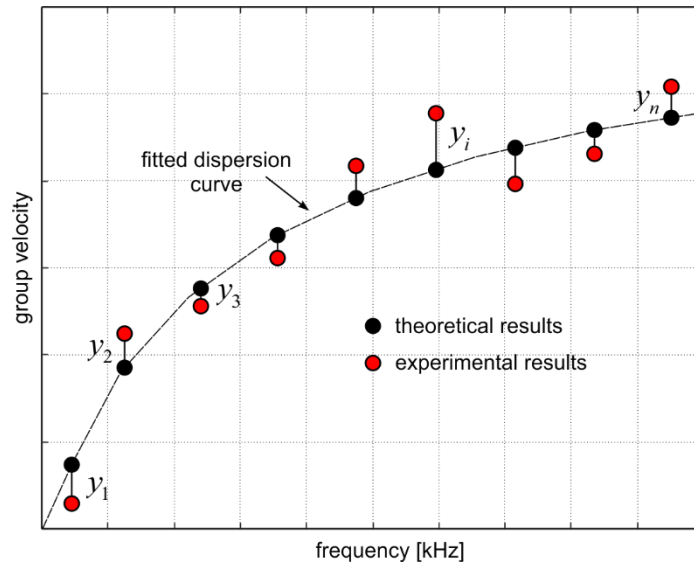
251 The second set of data was obtained from the experimental analysis:

$$252 \quad c_{gr}^E = \{(\Delta f, c_{gr}^E(\Delta f)), (2\Delta f, c_{gr}^E(2\Delta f)), \dots, (n\Delta f, c_{gr}^E(n\Delta c_{gr}))\} = \{(\Delta f, c_{gr}^{E,1}), (2\Delta f, c_{gr}^{E,2}), \dots, (n\Delta f, c_{gr}^{E,n})\}$$

253 Next, the value of the following function has been calculated:

$$254 \quad Y(d) = \frac{1}{n} \sum_{i=1}^n (y_i(d))^2 = \frac{1}{n} \sum_{i=1}^n (c_{gr}^{T,i}(d) - c_{gr}^{E,i})^2 \quad (10)$$

255 The calculations were performed for a varying plate thickness. The function  $Y(d)$  reached  
 256 the minimum value for the best matching of numerical and experimental dispersion curves  
 257 (Figure 5).



258

259

Figure 5 Matching of experimental and analytical results

260

261

262

263

264

265

266

267

268

269

270

271

272

273

274

275

276

In general, one can say that a similar effect in the form of a dispersion curve can be easily obtained using different excitation types i.e., broadband pulse excitation providing triggering multiple frequencies at the same time. This approach has been widely tested in corrosion assessment applications and its effectiveness in dispersion curve reconstruction based on Short Time Fourier Transform has been demonstrated. However, the broadband pulse excitation has several disadvantages which caused to decide to employ narrowband excitation. First of all, simultaneous excitation of several frequencies is associated with multiple wave mode excitation and further conversions. In the case of the specimens with more complex geometry and several modes varying in carrier frequency and velocity, it would be difficult to extract the part of the signal which should be processed. The second important reason is the possible application in real monitoring systems. Narrowband excitation associated usually with one single wave mode is much more effective in the detection of localized damage like corrosion pits or cracks. It is particularly important as long these two types of corrosion damage can occur simultaneously. Despite the fact this paper considers only general corrosion, the application of narrowband excitation potentially allows for both general corrosion degradation assessment (Zima et al., 2022), as well as the detection and localization of other damage types (Zima, 2021).

### 277 3 Experimental study

278

279

280

281

The experimental analysis of a stiffened steel plate was conducted, which is considered a primary structural component of the ship hull girder (Figure 6). The analysed stiffened plate was of 5 mm thickness, and its geometry is presented in Figure 6. The mechanical properties were determined via tensile tests of coupon specimens according to ISO standard (ISO, 2009).

282 The mean value from seven samples was estimated for the elastic modulus of 198 GPa and  
283 yield stress of 272.3 MPa.

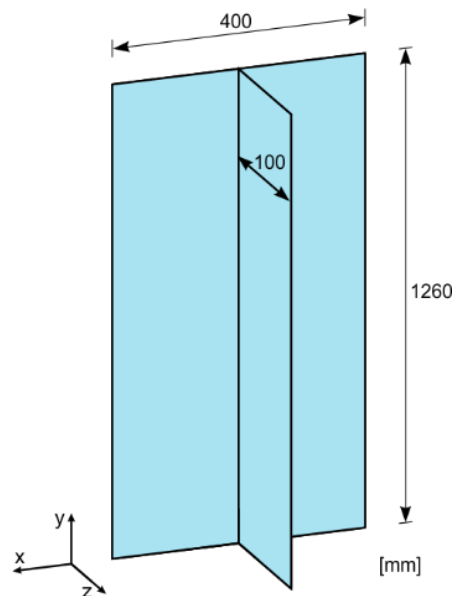


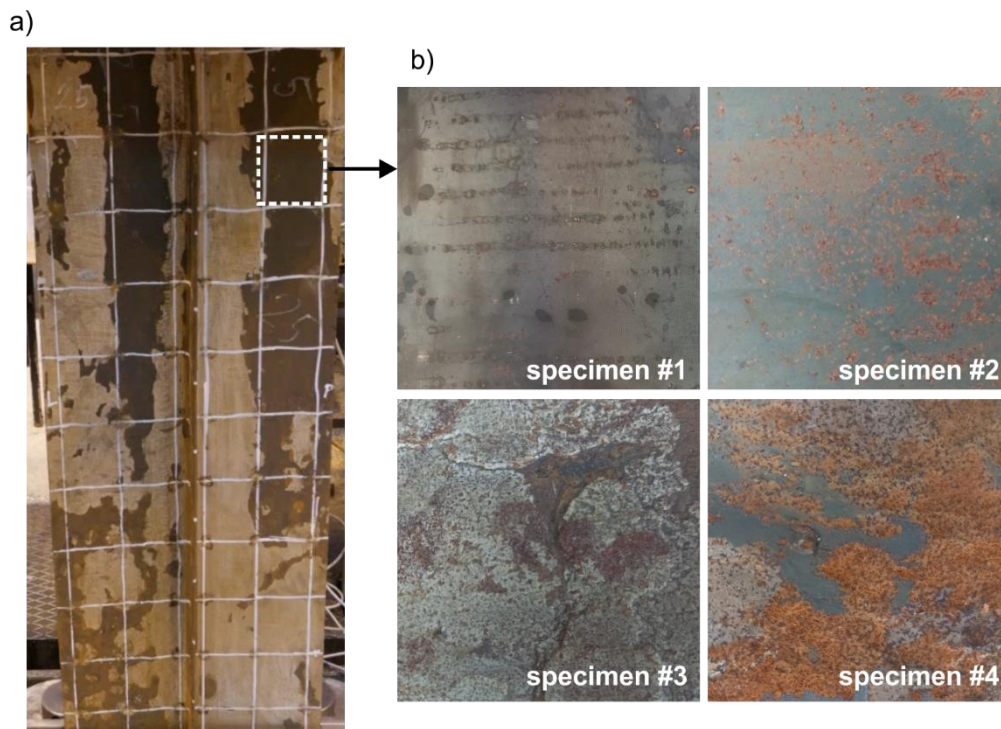
Figure 6. Stiffened plate geometry.

### 286 3.1 Corrosion degradation

287 The corrosion testing set-up was presented in (Woloszyk et al., 2021), together with the  
288 analysis of the generated corrosion degradation. The accelerated marine immersed corrosion  
289 degradation was generated by controlling the most important natural factors without applying  
290 DC. The specimens were placed in a 900-litre tank made from glass-reinforced plastic. The  
291 controlled environmental factors were the salinity (35 ppm), water circulation (induced by the  
292 circulation pumps), temperature (approx. 35 °C, increased by heaters), and dissolved oxygen  
293 content (augmented by the aeration pump over the limit of fully saturated conditions). The  
294 periodical measurements of the stiffened plate specimen's mass were carried out using the scale  
295 with an accuracy of 2 g. Based on that, the propagation of each specimen's mean value corrosion  
296 diminution with the time was determined. The mean corrosion rate obtained for 5 mm  
297 specimens was equal to 0.774 mm/year, and the total duration of the corrosion tests was 428  
298 days. In comparison to long-lasting experiments in natural seawater conditions, accelerated  
299 testing was a very efficient method. In real ship structures, the mean corrosion rate of the  
300 structures does not exceed the level of 0.1 mm/year (Melchers, 2008).

301 Three specimens of an initially 5 mm thickness were corroded, and three different  
302 degradation levels (calculated as the percentage loss of the initial mass of the specimen) were  
303 generated namely: 7%, 14% and 21%, by pulling the samples out of the water at different times.  
304 Although plate surfaces of different initial thicknesses were also corroded, the 5 mm plates

305 were chosen for validation of the new methodology. The thickness variability increased with  
306 the corrosion degradation level growth. Figure 7a shows the most severely corroded specimen,  
307 while Figure 7b presents the surfaces of any particular specimens.



308  
309 Figure 7 Corroded specimens: a) specimen with 21 % degradation level and b) surfaces of corroded specimens

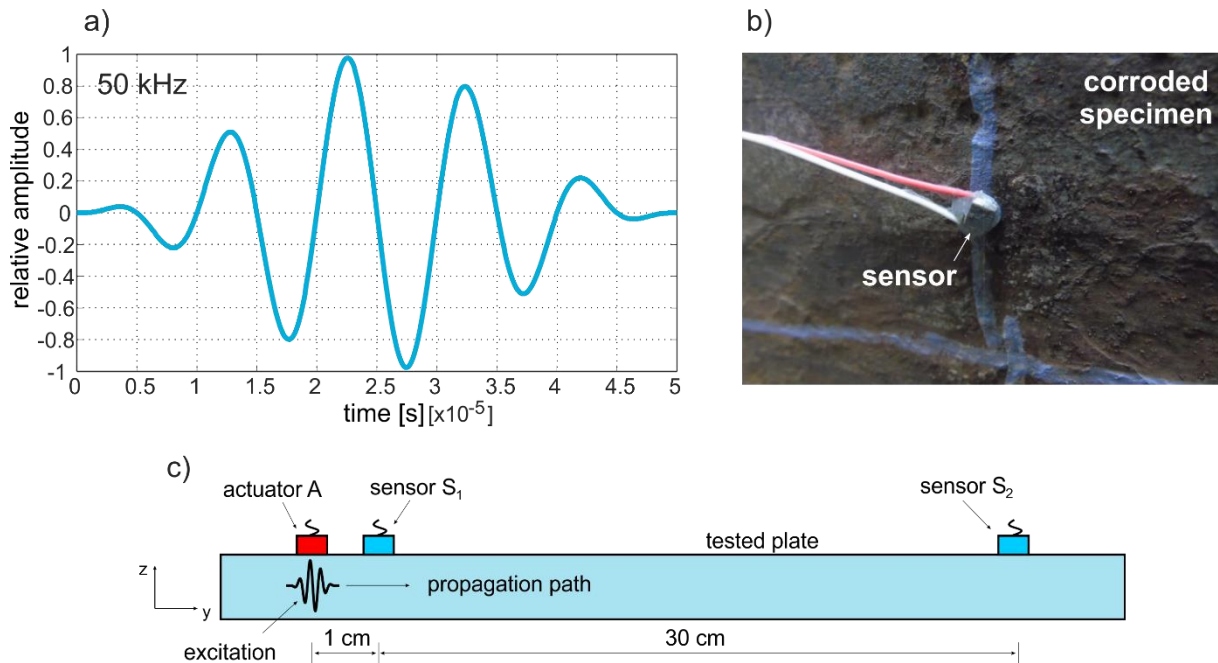
310  
311 It must be mentioned here that between environmental accelerated corrosion and the actual  
312 corrosion process some differences may occur, especially concerning the internal  
313 microstructure of the corroded element. However, the current study is mainly focused on the  
314 guided wave-based diagnostics method and recent studies (Zima, 2022) proved that the wave  
315 propagation velocity, as well as the time course of the signals, are dependent only on specimen  
316 thickness distribution. It means that two specimens varying in geometry but with the same  
317 thickness distribution will result in the same velocity and shape of the incident wave. Thus, the  
318 speed of the corrosion process has no direct influence on wave propagation signals but the  
319 resulting thickness variability and differences in specimen geometry may affect signal  
320 characteristics.

### 321 3.2 Guided wave propagation

322 The excitation and measurements of elastic waves were carried out by an experimental  
323 set-up comprised of an oscilloscope, function generator and piezoelectric transducers Noliac  
324 NAC2024. To improve the signal-to-noise ratio, the receiver was connected to the high voltage

325 amplifier ThorLab. The Lamb wave excitation was realised as a wave packet consisting of a  
 326 five-cycle sine modulated by a Hann window. The carrier frequency was from 50 to 250 kHz  
 327 with a step of 50 kHz (Figure 8a). The proposed algorithm has been tested for a low-frequency  
 328 range to avoid the excitation of the higher-order modes. The sampling frequency was 500 MHz,  
 329 and the input voltage was 20 V. To minimise the influence of electrical noises in the amplifier,  
 330 each signal was averaged 1024 times. The perpendicular excitation is associated with triggering  
 331 the propagation of flexural waves. Despite that, the presented reasoning is also valid for  
 332 symmetric modes, from practical reasons it is much easier to attach the transducer at the plate  
 333 surface rather than at the free edge. Therefore, further analysis concerns the antisymmetric  
 334 Lamb modes defined by Eq. (1b).

335 The first signal was captured at 10 mm from the excitation source, while the second was  
 336 310 mm. The distance  $x$  between sensors was 300 mm (Figure 8c).



337  
 338 Figure 8 Experimental tests: a) excitation functions and b) sensor attached at the corroded plate surface, c)  
 339 configuration of the transducers

340 The waves were propagated along the longer edge of the specimen (the propagation path  
 341 was parallel to the stiffener). Such placement of the transducers allowed for avoiding the  
 342 interference of reflections from edges and from stiffener with an incident wave which is further  
 343 processed. Indeed, the influence of the additional structural elements should be included in  
 344 further research. However, because the main aim of the present study is to develop and test the  
 345 novel procedure of the corrosion degradation level assessment, we have used the favourable  
 346 configuration of the transducers.

347 The reconstructed dispersion curve allows for assessing the corrosion degradation level  
 348 along the propagation path. The longer the distance, the greater the monitored area, and the  
 349 corrosion's thickness variability will be estimated as an equivalent average plate thickness.

350 The newly developed approach was tested in dispersion curve reconstruction on shorter  
 351 distances not exceeding a few centimetres. The short distance minimises the dispersion effects  
 352 and allows for a better characterisation of the corroded plate thickness variability as an  
 353 equivalent average plate thickness. However, in large-scale offshore or ship structures,  
 354 attaching sensors very close to each other would be inefficient. The distance of 30 cm was  
 355 chosen to compromise the size of the monitored area of the stiffened plate and the resolution of  
 356 the corrosion degradation plate surface roughness. Testing of more extended objects is possible  
 357 with adequate amplifying of the excitation. It is also possible to use a different approach like  
 358 multiple inputs-multiple outputs and a comprehensive sensor network to increase the monitored  
 359 area.

360

#### 361 **4 Analysis and results**

362 Wave propagation signals were processed to estimate the group propagation velocity for  
 363 various frequencies and determine the average corroded plate thickness along the propagation  
 364 path. The analysis was implemented in a MATLAB environment, and the adopted filtering  
 365 parameters are summarised in Table 1.

366 Table 1 Parameters of the Gaussian filters

excitation frequency [kHz]	frequency limits [kHz]		filter bandwidth	filters number
	$f_L$	$f_H$	$\Delta B$ [kHz]	$K$ [-]
50	35	65	20	11
100	70	130	40	11
150	100	200	50	11
200	130	260	60	11
250	160	330	60	11

367



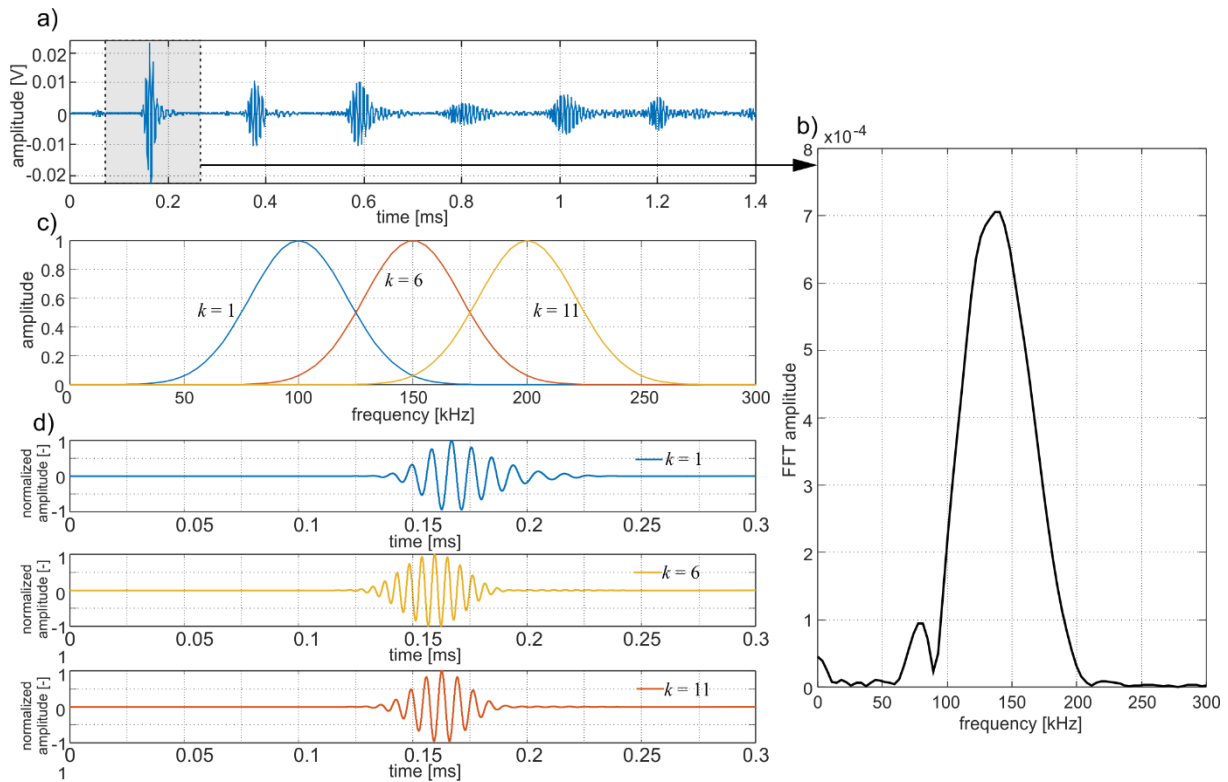


Figure 9 Signal processing: a) registered time-domain signal, b) Fourier transform of the extracted incident wave, c) filters and d) reconstructed signal after filtering

368  
369  
370

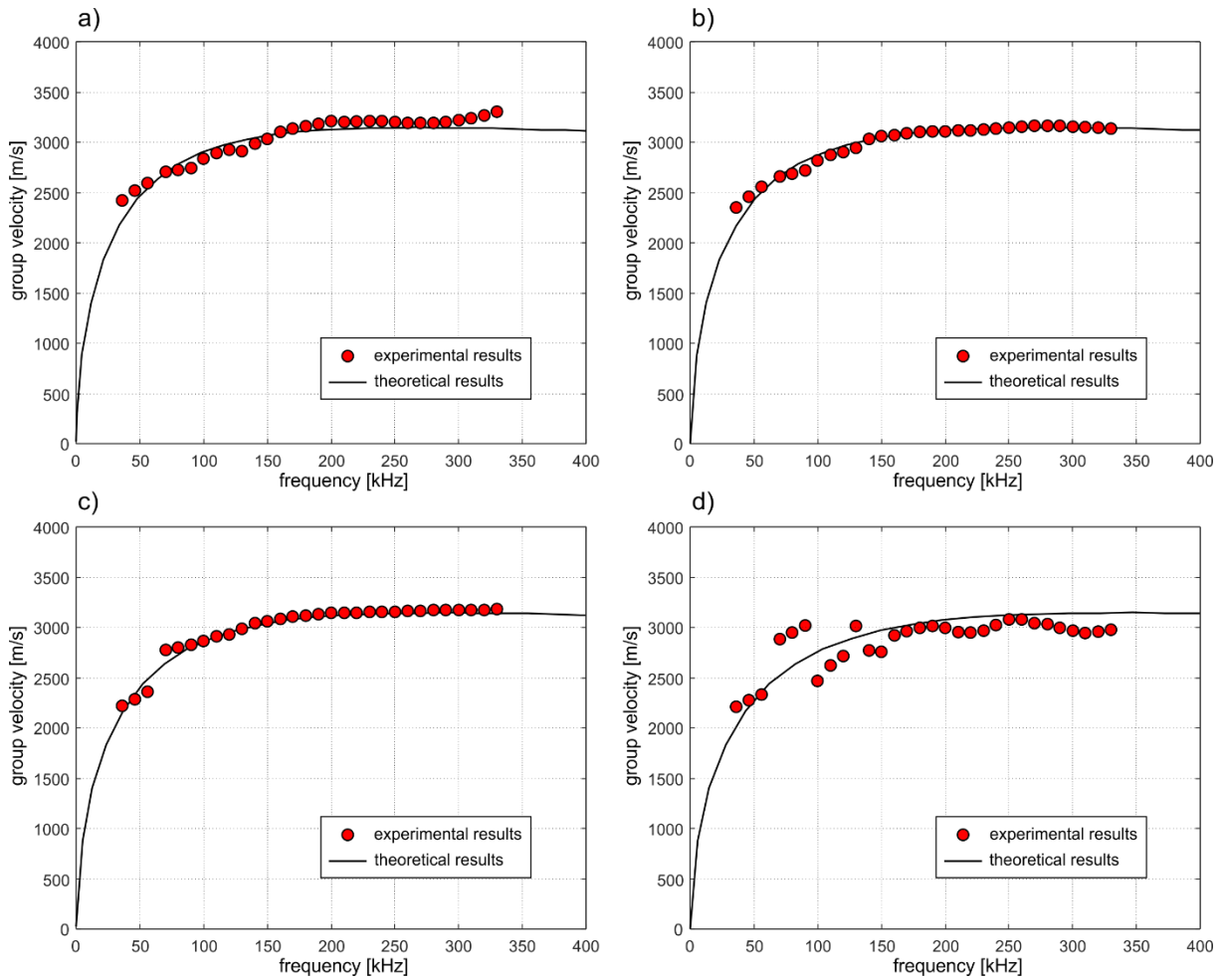
371 An exemplary signal captured by sensor S2 registering for the corroded plate (corrosion  
372 degradation level 7%) and the excitation frequency of 150 kHz, as well as the intermediate  
373 results in the form of a Fourier spectrum, filters, and three signals obtained for  $k$  equals to 1, 6  
374 and 11 are presented in Figure 9.

375 The analysis has been divided into two stages. The dispersion curve has been  
376 reconstructed within the first stage based on the ten signals registered for five different  
377 frequencies. Thus, in total, ten signals were processed. In the second stage, the dispersion curve  
378 has been determined based on only two adjacent signals registered for one frequency.

#### 379 4.1 Dispersion curve reconstruction based on several excitation frequencies

380 Figure 10 presents the results of reconstructing the dispersion curves for any particular  
381 specimens. Experimental outcomes are denoted by red dots, while the solid black line depicts  
382 the Lamb dispersion curve characterised by the minimal value of  $Y(d)$  (Eqn 10). Despite the  
383 experimental group velocity coinciding well with the dispersion curve, the difference in  
384 matching the analytical solution is visible, confirming the correctness of the proposed algorithm  
385 of dispersion curve reconstruction. The most significant deviation of experimental results from  
386 the theoretical curve was obtained for the specimen characterised by the highest corrosion  
387 degradation level (Figure 10d), which the more intense wave integration may cause with

388 irregularities of the corroded surface, as well as with the most significant deviation of the plate  
 389 thickness from the average value.



390  
 391 Figure 10 Reconstruction of dispersion curves for a) specimen #1, b) specimen #2, c) specimen #3 and d)  
 392 specimen #4

393 The estimated parameters of the analysed corroded plates are summarised in Table 2. The  
 394 estimated corrosion level  $C_a$  has been calculated based on the determined plate thickness from  
 395 the fitted dispersion curve:

396 
$$C_a = \frac{d_t}{d} \cdot 100\% , \quad (11)$$

397 where  $d$  is the thickness of the uncorroded plate determined non-destructively, and  $d_t$  is the  
 398 thickness of the corroded plate, where  $d$  was estimated as 5.18 mm. Comparing the results for  
 399 corroded and uncorroded plates, it can be seen that the guided wave propagation approach limits  
 400 the inaccuracies of determination of propagation velocity caused by the chosen method of the  
 401 time-of-flight calculation and the influence of deviation of material parameters. On the other  
 402 hand, the reference signals registered for the original structure are required for such comparison.  
 403 Still, it can be noticed that the reference measurement does not have to be made on the same  
 404 structure.

405 The estimated corrosion degradation levels differ slightly from the actual one, but a good  
 406 agreement between the results is observed. The absolute error, which is defined as the difference  
 407 between the accurate and estimated equivalent average thickness:

$$408 \quad e_a = |d_a - d_t| \quad (13)$$

409 did not exceed 0.5 mm, which indicates that the plate thickness may be estimated with high  
 410 accuracy even without reference measurements. The maximum value of the relative error  
 411 referencing to actual thickness:

$$412 \quad e_r = \frac{e_a}{d_a} \cdot 100\% , \quad (14)$$

413 is equal to 10.42% and was obtained for specimen #3 but is can be explained by the fact that  
 414 the general corrosion is not associated with perfect uniform thickness reduction. The higher  
 415 corrosion level  $C_d$  does not exclude that in some regions the thickness reduction is smaller and  
 416 opposite.

417 Table 2 Average corrosion degradation level of stiffened plates

specimen	actual corrosion level $C_d$ [%]	average thickness $d_a$ [mm]	thickness determined by Lamb waves $d_t$ [mm]	estimated corrosion level $C_a$ [%]	absolute error $e_a$ [mm]	relative error $e_r$ [%]
#1	0	5	5.180	0	0.180	2.40
#2	7	4.638	4.890	4.500	0.252	5.43
#3	14	4.320	4.770	6.835	0.450	10.42
#4	21	3.948	4.000	21.875	0.052	1.32

418

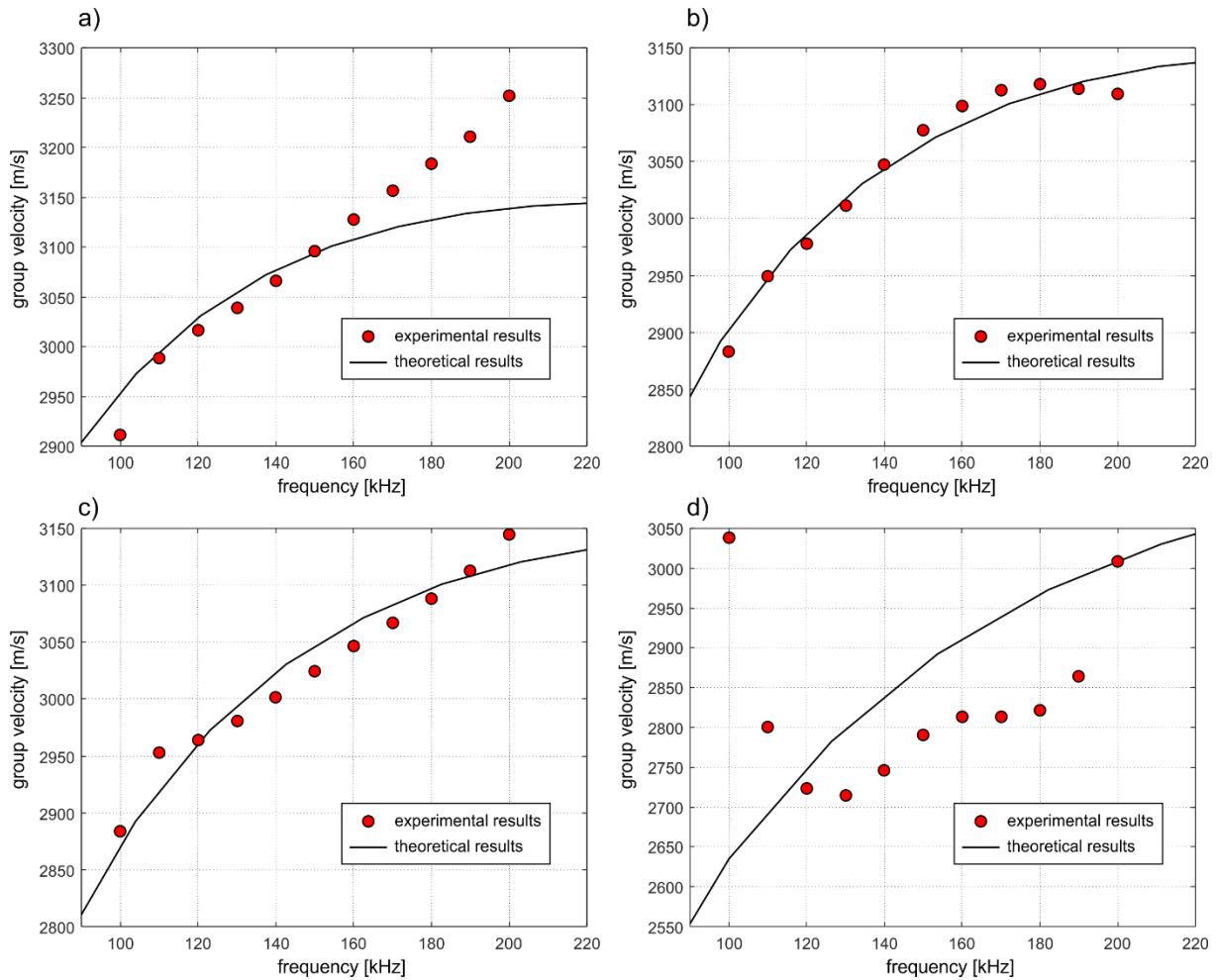
#### 419 4.2 Dispersion curve reconstruction based on one excitation frequency

420 An attempt of corrosion degradation assessment based on one excitation frequency and  
 421 only one pair of signals captured at points S1 and S2 were made. The segment of the dispersion  
 422 curve has been reconstructed based on the measurement made for an excitation frequency of  
 423 150 kHz. Based on the theoretical solution traced for uncorroded plate (Figure 2), one can  
 424 conclude that relatively low frequencies (<100 kHz) are highly dispersive, which means that  
 425 low-frequency change results in a significant alteration in the propagation velocity.  
 426 Consequently, the shape of the propagating wave packet varies significantly along the  
 427 propagation path. The potential inaccuracies in measuring the distance between sensors or  
 428 calculating the flight time result in a substantial over-or underestimation of the propagation  
 429 velocity. Despite that this frequency range seems to be sensitive to plate thickness changes, the  
 430 reconstruction of the dispersion curve may be laden with a substantial error.

431 In turn, for the high frequencies ( $>200$  kHz), the dispersion curve becomes flat, the  
432 velocity for various frequencies is similar, and the shape of the propagating wave packet  
433 remains unchanged. Moreover, the higher the frequency, the shorter the wave becomes and thus  
434 is much more sensitive to the surface irregularities caused by corrosion degradation. In the  
435 signal, additional reflections are registered, which hinders the unambiguous indication and  
436 further extraction of incident waves for the analysis. The wave energy is dissipated faster, and  
437 the SNR decreases. Moreover, one can see that the higher frequencies become insensitive to  
438 the thickness reduction. The plate thickness reduction is associated with an insignificant  
439 propagation velocity change. Considering all aspects mentioned above, a "medium" frequency  
440 of 150 kHz is used, which is a compromise between dispersion effects, SNR, and sensitivity to  
441 corrosion damage.

442 Figure 11 depicts the experimental group velocities and reconstructed dispersion curves,  
443 while the corrosion degradation level assessment is summarised in Table 3. The corrosion  
444 degradation level assessment accuracy is lower when the curve is traced based on only one  
445 measurement. However, still, a good agreement between actual and estimated corrosion  
446 degradation levels was noted. In all cases, the corrosion degradation level has been  
447 overestimated. However, the absolute error did not exceed 0.8 mm.

448 The most significant deviations of experimental outcomes from the theoretical solution  
449 are observed at the ends of the considered frequency range for the highest and the lowest  
450 frequency components of the fundamental antisymmetric mode (100 and 200 kHz). The main  
451 reason may be the presence of the side lobes, which were not eliminated from the frequency  
452 spectrum despite windowing the input signal and subsequent filtering the Fourier spectrum  
453 (Lyons, 2011). The same effect was also observed in the previous investigation stage for other  
454 frequencies. Still, the averaging of overlapping curve segments at the ends of the frequency  
455 range (Figure 4b) reduced the deviations from the theoretical curve.



456

457

458

Figure 11 Reconstruction of dispersion curves for a) specimen #1, b) specimen #2, c) specimen #3 and d) specimen #4

459

Table 3 Corrosion degradation level of stiffened plates

specimen	actual corrosion level $C_d$ [%]	average thickness $d_a$ [mm]	thickness determined by Lamb waves $d_t$ [mm]	estimated corrosion level $C_a$ [%]	absolute error $e_a$ [mm]	relative error $e_r$ [%]
#1	0	5	5.770	0	0.770	15.40
#2	7	4.638	5.170	10.399	0.532	11.47
#3	14	4.320	4.870	15.598	0.550	12.73
#4	21	3.948	3.290	42.981	0.658	16.67

460

### 4.3 Calibration and error mitigation

461

462

463

464

465

466

There are several different sources of inaccuracies where one of the most compelling reasons in the applied approach is the time of the flight. In this study, the time of flight was defined as a difference in the registration time of the peaks of the signal envelopes determined by using the cross-correlation method. However, there are many developed approaches for flight estimation, and the results differ slightly depending on which method was chosen (Xu et al., 2009). Because the thickness was overestimated in most cases, one can conclude a

467 systematic error made during the velocity determination. In the considered frequency range, the  
 468 increase of velocity is related to an increase in the thickness. Thus, possibly the applied method  
 469 of the time of flight determination based on cross-correlation of the Hilbert transform of  
 470 adjacent signals resulted in underestimating the registration time.

471 To investigate whether the systematic error of velocity determination influenced the  
 472 results, the following analysis has been conducted: based on the analytical and experimental  
 473 dispersion curves obtained for an undamaged plate with a known thickness of  $d = 5$  mm., the  
 474 error has been determined. The velocity overestimation was  $\Delta = 19$  m/s. The velocities obtained  
 475 for other stiffened plates have been reduced by  $\Delta$ , which means that the obtained curves were  
 476 just shifted down without changing their shapes, and then the procedure of the corrosion level  
 477 identification has been applied (Section 2.3). Table 4 contains the results obtained after  
 478 calibrating the velocity based on an uncorroded plate. It is visible that calibrating the velocity  
 479 increases the quality of the estimated corrosion degradation level. It is noted, that in most cases,  
 480 the presented method overestimates the thickness. However, for Specimen #4, the thickness is  
 481 underestimated. At that stage of development, this does not allow to make some general  
 482 conclusions regarding that issue and future studies are needed. The error influence may be  
 483 limited by conducting the measurements for various frequencies and various distances between  
 484 the transducers.

485 Table 4 Corrosion degradation level of stiffened plates after velocity calibration

specimen	actual corrosion level [%]	corrosion level estimated based on Lamb waves [%]	
		without velocity calibration	with velocity calibration
#1	0	0	0
#2	7	10.399	5.200
#3	14	15.598	9.500
#4	21	42.981	20.00

486

#### 487 4.4 Discussion

488 The results presented in the previous section confirm the proposed algorithm's  
 489 effectiveness in tracing the dispersion curve and identifying the averaged structural degradation  
 490 level. The main advantage over so far presented ultrasonic methods dedicated to thickness  
 491 estimation of corroded ship's structural components is the necessity to collect a limited number  
 492 of signals. The transducers network does not demand a large number of PZT. The actuator  
 493 triggered the signals was captured by two sensors and one actuator placed on a line. The first  
 494 sensor should be attached at a short distance from an actuator, which provides a high-amplitude

495 incident wave. The spatial distance between the sensors can be adjusted to the structure size,  
496 used equipment, and the desired accuracy of identifying the average corroded plate thickness.

497 A significant advantage is that the presented wave-based method does not require  
498 collecting the reference data for an uncorroded structure. The measurements of uncorroded  
499 plates improve the quality of the results obtained and allow for better corrosion degradation  
500 assessment by reducing the influence of systematic errors, but they are not indispensable.

501 The robustness of the novel procedure was examined in two stages. In the first stage, the  
502 group velocity dispersion curve has been reconstructed using signals registered for various  
503 excitation frequencies. The main advantage of the approach based on the measurement of  
504 several frequencies is that the shape of the dispersion curve can be faithfully reconstructed. On  
505 the other hand, the number of required signals and, in consequence, the time of analysis is  
506 longer. In the second stage, the signals were registered for only one excitation type. The main  
507 advantage of reconstructing only one chosen segment of the dispersion curve is the necessity to  
508 use only one excitation frequency for all tested specimens. The assessment of the corrosion  
509 degradation demands only two signals be captured at the known distance. However, it also  
510 demands the appropriate choice of excitation frequency, which is not a trivial issue and requires  
511 considering the shape of the dispersion curve determined based on an analytical equation.

512 Despite promising results, the indispensable prerequisite of the further enhancement of  
513 the proposed approach demanded before its practical application is the consideration of its  
514 limitations. First, the corrosion degradation identification algorithm does not take into account  
515 the plate thickness variability. The corrosion degradation level was indirectly averaged by  
516 assuming that the thickness is constant along the propagation path. However, the plate thickness  
517 variability can be mapped much better by extending the sensors network or taking additional  
518 measurements at other points.

519 The irregularities of the corroded surfaces influenced the quality of the results. The  
520 disturbance interactions with abnormalities resulting in wave diffractions and conversions lead  
521 to incident wave indication and extraction difficulties for further analysis. Though only one  
522 antisymmetric wave mode could propagate within the considered frequency range, wave  
523 integration with irregular surfaces might also induce low-energy symmetric wave mode.  
524 Propagating of multiple wave packets and their interference affects the shape of the incident  
525 wave and, in consequence, the characteristics of the frequency spectrum, which led to  
526 inaccuracies in time of flight estimation.

527 The discrepancies between theoretical and experimental results can also originate from  
528 the assumption about the constant value of elastic modulus and material density; however, the

529 material parameters are also predefined in standard ultrasonic thickness measurement to  
530 calculate the velocity of the pressure wave. Thus, further development of the corrosion  
531 degradation level identification algorithm may include the impact on material parameters or  
532 fluctuations on the dispersion curve shape. The dependence between wave velocity and any  
533 parameter in the dispersion Lamb equation is strongly nonlinear, which means that, e.g., the  
534 overestimation of elastic modulus may lead to overestimating wave velocity for one excitation  
535 frequency and underestimating for other frequencies. It should be noted that the influence of  
536 corrosion degradation on material properties was not considered here. The density, Poisson's  
537 ratio, and elastic modulus were assumed the same for all analysed stiffened plates.

538 The next element necessary to consider in further studies is the influence of the additional  
539 structural elements affecting wave propagation. The problem of the additional reflections can  
540 be solved in two different ways. In general, guided wave-based algorithms are usually used for  
541 processing the data collected by specially designed SHM systems. In such cases, signals are  
542 measured for various states of the investigated specimen and the reference measurements are  
543 available for the investigators. Particular reflections can be identified and interpreted and next  
544 excluded on the further stages of monitoring and signal processing. The second way to limit the  
545 problem of additional reflections from boundaries and stiffeners is the utilization of different  
546 transducer types. Recently, a novel type of frequency steerable transducers has been developed.  
547 The novel transducer allows sending of the signal only in one chosen direction, which is  
548 dependent on the excitation frequency (Baravelli et al., 2013; De Marchi et al., 2016). The main  
549 lobe, characterized by high amplitude propagates in one direction while small-amplitude side  
550 lobes propagate in other directions. Even if the total elimination of the boundaries reflections  
551 is not possible, their amplitudes can be significantly reduced by focusing wave energy only in  
552 an interesting direction.

## 553 **5 Future perspectives**

554 Since the present study mainly focused on the development of the signal processing which  
555 can be potentially used in the SHM systems, several aspects were not considered here and  
556 should be investigated in future studies, including:

- 557 • Ships and offshore structures are large in size and complex in geometry. Their  
558 diagnostics would require a more complex sensor network. The optimal sensor  
559 placement will be considered. The trade-off between the resolution and extent of the  
560 sensors network must be considered.
- 561 • Practical application of the developed approach requires considering the reliability of the  
562 proposed method and the influence of inaccuracies on the determined DoD (Falcetelli et



563 al., 2021). This should in particular cover further studies regarding higher thicknesses of  
564 analysed plates and related uncertainty levels.

565 • Guided waves are widely used for localized damage detection. Therefore, the possibility  
566 of building multi-step algorithms for both general uniform and pitting corrosion detection  
567 and evaluation must be investigated.

## 568 **6 Conclusions**

569 This study conducted theoretical and experimental investigations of guided wave  
570 propagation in corroded stiffened plates. The newly developed approach allows for an average  
571 corrosion degradation level identification based on the single measurements of the tested  
572 stiffened plates.

573 The experimental data acquired for four different stiffened plates varying in degradation  
574 level confirmed the correctness of the developed procedure of dispersion curve reconstruction.  
575 The corrosion degradation level identification has been made in several different ways: once  
576 the dispersion curve has been traced based on several measurements made for various  
577 frequencies. At the same time, in the second case, the signals were captured for only one  
578 excitation type. It was proved that the corrosion degradation level was better assessed if the  
579 measurements involved a wider frequency range. However, regardless of the considered  
580 frequency range within the dispersion curve that has been reconstructed, the corrosion  
581 degradation level remained slightly underestimated, which indicated the possible systematic  
582 error related to the time of flight and, in consequence, with group velocity estimation. Based on  
583 the assumption that the initial thickness of the uncorroded stiffened plate is usually known a  
584 priori, the value of systematic error has been established and included in further assessing the  
585 corrosion deterioration of other stiffened plates. It allowed for a better estimation of the precise  
586 degree of corrosion degradation.

587 The highest deviation between experimental measurements and theoretically defined  
588 dispersion curve was observed for the most severely corroded stiffened plates. This allows the  
589 hypothesis that the presented methodology could determine the average thickness and its  
590 variability level. After further development, the proposed method should be applicable in all  
591 cases requiring multiple ultrasonic measurements to assess the thickness of steel structural  
592 elements.

## 593 **Acknowledgement**

594 The first author greatly acknowledges the support of the Foundation for Polish Science (FNP).

596

597

**References**

- 598 Baravelli E, Senesi M, Ruzzene M, De Marchi L. Fabrication and Characterization of a Wavenumber-Spiral  
599 Frequency-Steerable Acoustic Transducer for Source Localization in Plate Structures. *IEEE Trans Instrum Meas*  
600 2013;62:2197–204. <https://doi.org/10.1109/TIM.2013.2255992>.
- 601 Cao X, Zeng L, Lin J. Generalized scattering matrix method for Lamb wave scattering analysis at cascaded  
602 notches. *J Vib Control* 2021;107754632110377. <https://doi.org/10.1177/10775463211037790>.
- 603 Cegla F, Gajdacs A. Mitigating the effects of surface morphology changes during ultrasonic wall thickness  
604 monitoring. *AIP Conf. Proc.*, 2016, p. 170001. <https://doi.org/10.1063/1.4940624>.
- 605 Ciampa F, Scarselli G, Pickering S, Meo M. Nonlinear elastic wave tomography for the imaging of corrosion  
606 damage. *Ultrasonics* 2015;62:147–55. <https://doi.org/10.1016/j.ultras.2015.05.011>.
- 607 Ding X, Xu C, Deng M, Zhao Y, Bi X, Hu N. Experimental investigation of the surface corrosion damage in plates  
608 based on nonlinear Lamb wave methods. *NDT E Int* 2021;121:102466.  
609 <https://doi.org/10.1016/j.ndteint.2021.102466>.
- 610 Draudviliene L, Tumsys O, Mazeika L, Zukauskas E. Estimation of the Lamb wave phase velocity dispersion  
611 curves using only two adjacent signals. *Compos Struct* 2021;258:113174.  
612 <https://doi.org/10.1016/j.compstruct.2020.113174>.
- 613 Ervin BL, Kuchma DA, Bernhard JT, Reis H. Monitoring Corrosion of Rebar Embedded in Mortar Using High-  
614 Frequency Guided Ultrasonic Waves. *J Eng Mech* 2009;135:9–19. [https://doi.org/10.1061/\(ASCE\)0733-9399\(2009\)135:1\(9\)](https://doi.org/10.1061/(ASCE)0733-9399(2009)135:1(9)).
- 616 Ervin BL, Reis H. Longitudinal guided waves for monitoring corrosion in reinforced mortar. *Meas Sci Technol*  
617 2008;19:055702. <https://doi.org/10.1088/0957-0233/19/5/055702>.
- 618 Falcetelli F, Yue N, Di Sante R, Zarouchas D. Probability of detection, localization, and sizing: The evolution of  
619 reliability metrics in Structural Health Monitoring. *Struct Heal Monit* 2021;147592172110607.  
620 <https://doi.org/10.1177/14759217211060780>.
- 621 Farhidzadeh A, Salamone S. Reference-free corrosion damage diagnosis in steel strands using guided ultrasonic  
622 waves. *Ultrasonics* 2015;57:198–208. <https://doi.org/10.1016/j.ultras.2014.11.011>.
- 623 Flashback history: Tanker Prestige sinking (Video). 2015.
- 624 Howard R, Cegla F. Detectability of corrosion damage with circumferential guided waves in reflection and  
625 transmission. *NDT E Int* 2017;91:108–19. <https://doi.org/10.1016/j.ndteint.2017.07.004>.
- 626 Hu M, He J, Zhou C, Shu Z, Yang W. Surface damage detection of steel plate with different depths based on Lamb  
627 wave. *Measurement* 2022;187:110364. <https://doi.org/10.1016/j.measurement.2021.110364>.
- 628 Hua J, Cao X, Yi Y, Lin J. Time-frequency damage index of Broadband Lamb wave for corrosion inspection. *J*  
629 *Sound Vib* 2020;464:114985. <https://doi.org/10.1016/j.jsv.2019.114985>.
- 630 ISO. Metallic materials - Tensile testing - Part 1: Method of test at room temperature. *Int Stand ISO 6892-1* 2009.
- 631 Lamb H. On waves in an elastic plate. *Proc R Soc London Ser A, Contain Pap a Math Phys Character* 1917;93:114–  
632 28. <https://doi.org/10.1098/rspa.1917.0008>.

- 633 Li Z, Wang Y, Zheng J, Liu N, Li M, Teng J. Stress measurement for steel slender waveguides based on the  
634 nonlinear relation between guided wave group velocity and stress. *Measurement* 2021;179:109465.  
635 <https://doi.org/10.1016/j.measurement.2021.109465>.
- 636 Lyons R. *Understanding Digital Signal Processing*. 3rd ed. Prentice-Hall; 2011.
- 637 De Marchi L, Testoni N, Marzani A. A New Generation of Frequency Steerable Transducers for Lamb Waves  
638 Inspections. 19th World Conf. Non-Destructive Test. (WCNDT 2016), Munich: 2016, p. 1–8.
- 639 Melchers RE. Development of new applied models for steel corrosion in marine applications including shipping.  
640 *Ships Offshore Struct* 2008;3:135–44. <https://doi.org/10.1080/17445300701799851>.
- 641 Moustafa A, Niri ED, Farhidzadeh A, Salamone S. Corrosion monitoring of post-tensioned concrete structures  
642 using fractal analysis of guided ultrasonic waves. *Struct Control Heal Monit* 2014;21:438–48.  
643 <https://doi.org/10.1002/stc.1586>.
- 644 Panayotova M, Garbatov Y. Corrosion of steels in marine environment, monitoring and standards. *Saf. Reliab.*  
645 *Ind. Prod. Syst. Struct.*, CRC Press; 2010, p. 369–413. <https://doi.org/10.1201/b10572-36>.
- 646 Parunov J, Senjanović I, Guedes Soares C. Hull-girder reliability of new generation oil tankers. *Mar Struct*  
647 2007;20:49–70. <https://doi.org/10.1016/j.marstruc.2007.03.002>.
- 648 Ping He. Simulation of ultrasound pulse propagation in lossy media obeying a frequency power law. *IEEE Trans*  
649 *Ultrason Ferroelectr Freq Control* 1998;45:114–25. <https://doi.org/10.1109/58.646916>.
- 650 Sharma S, Mukherjee A. Longitudinal Guided Waves for Monitoring Chloride Corrosion in Reinforcing Bars in  
651 Concrete. *Struct Heal Monit* 2010;9:555–67. <https://doi.org/10.1177/1475921710365415>.
- 652 Tian Z, Xiao W, Ma Z, Yu L. Dispersion curve regression – assisted wideband local wavenumber analysis for  
653 characterizing three-dimensional (3D) profile of hidden corrosion damage. *Mech Syst Signal Process*  
654 2021;150:107347. <https://doi.org/10.1016/j.ymssp.2020.107347>.
- 655 Wandowski T, Malinowski P, Ostachowicz WM. Damage detection with concentrated configurations of  
656 piezoelectric transducers. *Smart Mater Struct* 2011;20:025002. <https://doi.org/10.1088/0964-1726/20/2/025002>.
- 657 Woloszyk K, Garbatov Y, Kowalski J. Indoor accelerated controlled corrosion degradation test of small- and large-  
658 scale specimens. *Ocean Eng* 2021;241:110039. <https://doi.org/10.1016/j.oceaneng.2021.110039>.
- 659 Woloszyk K, Kahsin M, Garbatov Y. Numerical assessment of ultimate strength of severe corroded stiffened  
660 plates. *Eng Struct* 2018;168:346–54. <https://doi.org/10.1016/j.engstruct.2018.04.085>.
- 661 Xiao L, Peng J, Zhang J, Ma Y, Cai CS. Comparative assessment of mechanical properties of HPS between  
662 electrochemical corrosion and spray corrosion. *Constr Build Mater* 2020;237:117735.  
663 <https://doi.org/10.1016/j.conbuildmat.2019.117735>.
- 664 Xu B, Yu L, Giurgiutiu V. Advanced methods for time-of-flight estimation with application to Lamb wave  
665 structural health monitoring. *Proc. 7th Int. Work. Struct. Heal. Monit.*, Palo Alto, CA, USA: 2009.
- 666 Yuan Y, Ji Y, Shah S. Comparison of Two Accelerated Corrosion Techniques for Concrete Structures. *ACI Struct*  
667 *J* 2007;104:344–7. <https://doi.org/10.14359/18624>.
- 668 Zayed A, Garbatov Y, Guedes Soares C. Corrosion degradation of ship hull steel plates accounting for local

- 669 environmental conditions. *Ocean Eng* 2018;163:299–306. <https://doi.org/10.1016/j.oceaneng.2018.05.047>.
- 670 Zayed A, Garbatov Y, Guedes Soares C. Non-destructive Corrosion Inspection Modeling of Tanker Structures.  
671 Vol. 2 Struct. Saf. Reliab., ASMEDC; 2008, p. 465–76. <https://doi.org/10.1115/OMAE2008-57500>.
- 672 Zima B. Determination of stepped plate thickness distribution using guided waves and compressed sensing  
673 approach. *Measurement* 2022;196:111221. <https://doi.org/10.1016/j.measurement.2022.111221>.
- 674 Zima B. Damage detection in plates based on Lamb wavefront shape reconstruction. *Measurement*  
675 2021;177:109206. <https://doi.org/10.1016/j.measurement.2021.109206>.
- 676 Zima B, Rucka M. Guided wave propagation for assessment of adhesive bonding between steel and concrete.  
677 *Procedia Eng* 2017;199:2300–5. <https://doi.org/10.1016/j.proeng.2017.09.189>.
- 678 Zima B, Woloszyk K, Garbatov Y. Corrosion degradation monitoring of ship stiffened plates using guided wave  
679 phase velocity and constrained convex optimization method. *Ocean Eng* 2022;253.
- 680